Pergamon

Int. J. Heat Mass Transfer. Vol. 39, No. 7, pp. 1429–1438, 1996

0017-9310/96 $15.00 + 0.00

0017-9310(95)00180-8

Thermophoretic deposition including an application to the outside vapor deposition process

C. K. WU and R. GREIF†

Department of Mechanical Engineering, University of California at Berkeley, Berkeley, CA 94720, U.S.A.

(*Received* 1 *August* 1994 *and in final form* 9 *May* 1995)

Abstract—A study has been made of the flow, heat and mass transfer with chemical reactions and thermophoretic deposition with application to the outside vapor deposition (OVD) process. The system includes a flow that is emerging from a burner containing methane, oxygen, nitrogen and silicon tetrachloride and impinges on a cylindrical target. Silica soot particles are formed by the oxidation of silicon tetrachloride and the motion of the particles is determined from the combined effects of thermophoresis, buoyancy and the forced flow. The governing equations which include the effects of buoyancy, variable properties, chemical reactions and thermophoretic transport have been solved numerically for a slot burner and a long cylinder in a two-dimensional configuration. The effects of the separation distance between the burner and the target, the diameter and the rotational speed of the target and the eccentricity of the burner have been studied. The particle deposition flux and the deposition efficiency are investigated over a range of values of the parameters.

1. INTRODUCTION

The manufacture of optical fibers has been successfully carried out utilizing particle deposition techniques (Li [1]). In the outside vapor deposition (OVD) and vapor axial deposition (VAD) processes, $SiCl_4$, CH_4, O_2 and N_2 gases flow in a burner which is composed of concentric rings of discrete holes (OVD) or a series of concentric tubes (VAD). The gases leave the burner and impinge on a horizontal (OVD) or a vertical (VAD) oriented cylindrical target (Bautista and Atkins [2]). Oxidation and hydrolysis reactions take place in the gas stream and silica particles are formed and deposit on the target.

Homsy *et al.* [3] and Batchelor and Shen [4] analyzed the thermophoretic deposition of particles for a uniform flow past a cylinder based on the Blasius series solution. Garg and Jayaraj [5, 6] calculated the thermophoretic deposition over a cylinder for a specified pressure gradient of the external flow. These studies utilized boundary layer assumptions in conjunction with a simple external flow. Experimental results (Bautista *et al.* [7], Graham and Alam [8]) have shown that the variation of the flow and heat transfer on the surface of the cylinder, as well as the interaction between the burner and the target, have strong effects on the particle deposition. Alam *et al.* [9] investigated thermophoretic deposition for a plane jet impinging on a flat plate. Kang and Greif [10] investigated the thermophoretic transport for a jet impinging on a cylindrical target and included the effects of buoyancy and variable properties. Tsai and Greif [11] studied thermophoretic transport to a disk and included the effects of buoyancy and variable properties.

In most external deposition studies the effects of chemical reactions have been neglected. Tsai and Greif [12] have shown that chemical kinetics has an important influence on the thermophoretic deposition for a jet impinging on a disk. Silica particles are produced by the oxidation of silicon tetrachloride which is activated by the energy release from the oxidation of methane; these reactions are included in the present study. The particles deposit on a cylindrical target. Single step global reaction kinetics, buoyancy and variable properties are included in the analysis. A finite difference numerical method is used to solve the coupled mass, momentum, energy and species conservation equations.

2. ANALYSIS

2.1. *Coordinates and governing equations*

In external deposition processes, silica particles are produced in a reacting flow that leaves a burner. In Fig. 1(a) a burner is shown which consists of a central channel which contains a stoichiometric mixture of silicon tetrachloride and oxygen; the outer channels contain nitrogen, methane and oxygen, and nitrogen, respectively. The silica particles, which result from the oxidation of silicon tetrachloride, deposit on a circular cylindrical target.

A previous study of the OVD process specified a

† Author to whom correspondence should be addressed.

NOMENCLATURE

A_1 Arrhenius constant for the oxidation of methane, 8.3×10^5 [s^{-1}]
A_2 Arrhenius constant for the oxidation of silicon tetrachloride, 1.7×10^{14} [s^{-1}]
A_i convection–diffusion coefficients
$\vec{\mathbf{a}}^i$ contravariant base vector
b source term in the discretized equation
C concentration of the particles
C_f skin-friction coefficient, $2\tau_w/\rho_j U_j^2$
c_p specific heat at constant pressure
E_1 activation energy of methane oxidation, 126 kJ mol^{-1}
E_2 activation energy of silicon tetrachloride oxidation, 402 kJ mol^{-1}
F_w mass flux of the particles on the surface of the cylinder
g square of the Jacobian
g_v acceleration of gravity
g^{ij} components of the contravariant metric tensor
$\vec{\mathbf{i}}, \vec{\mathbf{j}}$ Cartesian base vectors
J_w deposition flux on the surface of the cylinder
K coefficient of the thermophoretic velocity
k conductivity
L distance between the nozzle and the cylinder
L_s separation length
M_i molecular weight of species i
p static pressure
q_w heat flux on the surface of the cylinder
R radius of a cylinder
R_u gas constant
S_ϕ source term in the governing equation
T temperature
U^i contravariant velocity component
U_j magnitude of the gas jet velocity
u, v Cartesian components of the velocity
Y_i mass fraction of i species
x, y Cartesian coordinate.

Greek symbols
Γ general diffusive coefficient
ΔH_i heat of reaction
η deposition efficiency
θ angle measured from the front stagnation point
μ viscosity
ν kinetic viscosity
ξ^i curvilinear coordinate, $\xi^1 = \xi$, $\xi^2 = \eta$
ρ density
ϕ general dependent variable
Ω rotational speed
ω_i reaction rate for reaction i.

Subscripts
N, S, E, W four nodes around the grid point P
a ambient value
j values at the torch exit
w values at the surface of the cylinder
ξ^i partial differentiation with respect to ξ^i.

distribution of particles at the exit from a burner and studied the fluid dynamics, heat and mass transfer and particle deposition but did not include chemical reactions (Kang and Greif [10]). To accurately determine the deposition rate and efficiency, full consideration must be given to chemical kinetics in addition to fluid, energy, species and thermophoretic transport mechanisms. The present study includes both methane and silicon tetrachloride oxidation reactions and uses single step chemical kinetics with Arrhenius rates. For methane oxidation, the reaction rate ω_1 given by Westbrook and Dryer [13] is:

$$CH_4 + 2O_2 \rightarrow CO_2 + 2H_2O,$$

$$\omega_1 = [CH_4]^{-0.3}[O_2]^{1.3} A_1 \exp\left(-\frac{E_1}{R_u T}\right). \quad (1)$$

For the oxidation of silicon tetrachloride, the reaction rate ω_2 used by Kim and Pratsinis [14] is:

$$SiCl_4 + O_2 \rightarrow SiO_2 + 2Cl_2,$$

$$\omega_2 = [SiCl_4] A_2 \exp\left(-\frac{E_2}{R_u T}\right). \quad (2)$$

The Reynolds number based on the burner width is approximately 100 and laminar flow is assumed. To accurately predict the local heat transfer and deposition on a cylinder [Fig. 1(b)], a two-dimensional (2D), C-type non-orthogonal curvilinear coordinate system is utilized to carry out the numerical calculations (Thompson *et al.* [15], Kang and Greif [10, 16]). The domain is transformed into the rectangular region shown in Fig. 1(c) where the branch cut is the center line of the wake. Two transformation functions $\xi(x, y)$ and $\eta(x, y)$ are obtained by solving Poisson equations. The governing equations for the gas phase written in conservative form in the non-orthogonal coordinate system are:

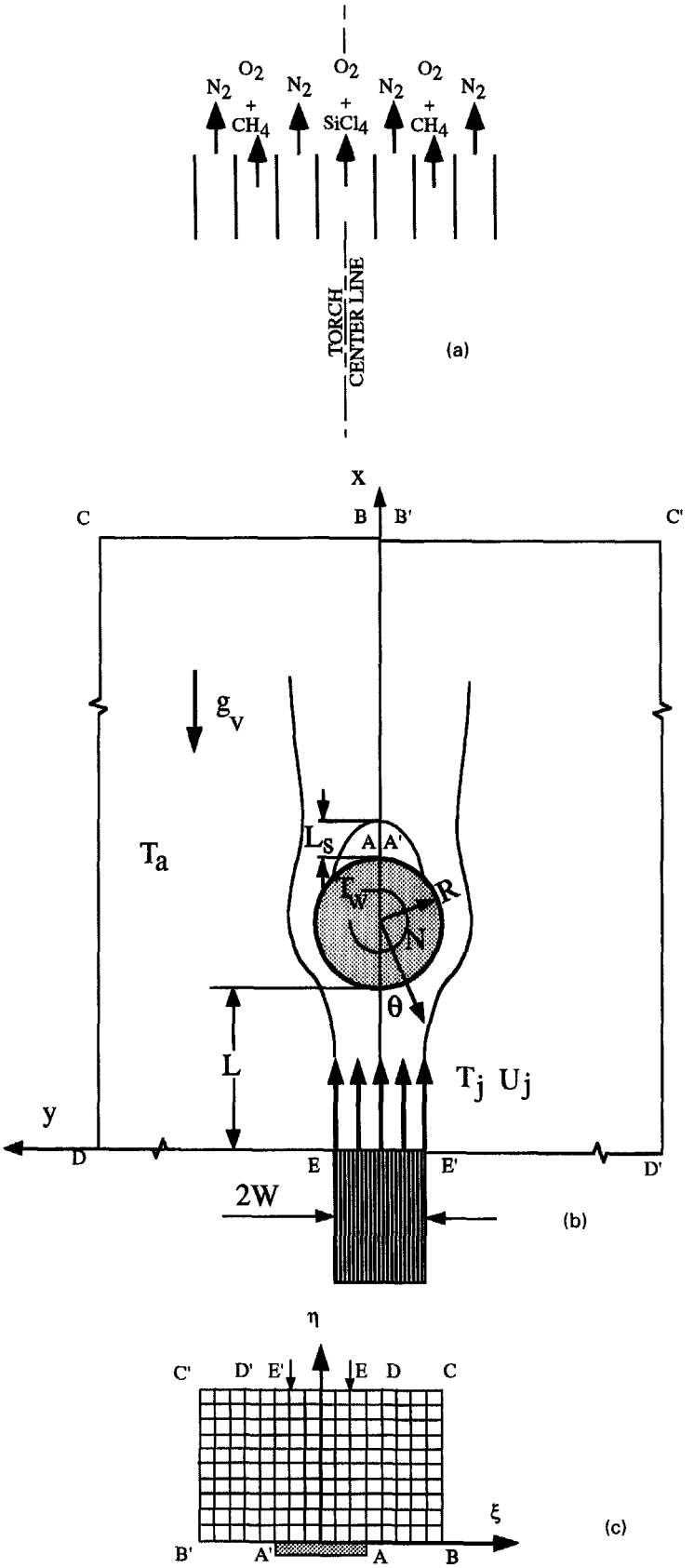

Fig. 1. (a) Configuration of the burner. (b) Flow configuration and coordinate system. (c) Transformed domain.

Continuity:

$$\sqrt{g}\rho_t + (\sqrt{g}\rho U^i)_{\xi^i} = 0 \tag{3}$$

X-momentum:

$$\sqrt{g}(\rho u)_t + [\sqrt{g}(\rho U^i u - \mu g^{ij} u_{\xi^j})]_{\xi^i} + (y_{\xi^2} p)_{\xi^1} - (y_{\xi^2} p)_{\xi^2} - \sqrt{g} g_v (\rho - \rho_a) = 0 \tag{4}$$

Y-momentum:

$$\sqrt{g}(\rho v)_t + [\sqrt{g}(\rho U^i v - \mu g^{ij} v_{\xi^j})]_{\xi^i} + (x_{\xi^2} p)_{\xi^1} - (x_{\xi^1} p)_{\xi^2} = 0 \tag{5}$$

Energy:

$$\sqrt{g}(\rho c_p T)_t + [\sqrt{g}(\rho c_p U^i T - k g^{ij} T_{\xi^j})]_{\xi^i} - \sqrt{g}\Delta H_k \omega_k = 0 \tag{6}$$

Species equations for the gas phase:

$$\sqrt{g}(\rho Y_l)_t + [\sqrt{g}(\rho U^i Y_l - \rho D_l g^{ij} Y_{l\xi^j})]_{\xi^i} - \sqrt{g}(v''_{lk} - v'_{lk})\omega_k M_l = 0, l = 1, 7 \tag{7}$$

where

$$\xi^1 = \xi, \xi^2 = \eta, U^i = \vec{a}^i \cdot (u\vec{i} + v\vec{j}),$$

$$\vec{a}^i = \vec{\nabla}\xi^i, g^{ij} = \vec{a}^i \cdot \vec{a}^j, \sqrt{g} = \frac{1}{\det|g^{ij}|} \tag{8}$$

and repeated subscripts refer to a summation. There are seven species (CH_4, O_2, CO_2, H_2O, $SiCl_4$, Cl_2 and N_2) and two reactions ($k = 1, 2$) for the gas phase that are considered. The mass fraction of nitrogen, Y_{N_2}, is obtained by applying the relation $\Sigma_{i=1}^{7} Y_i = 1$. The heats of reaction for methane and silicon tetrachloride oxidation are equal to 805 and 251 kJ mol^{-1}, respectively.

The density of the gas is determined using the ideal gas law at one atm thermodynamic pressure:

$$P = \rho \frac{R_u}{M} T, M = \left(\sum_{i=1}^{7} \frac{Y_i}{M_i} \right)^{-1}. \tag{9}$$

The viscosity and thermal conductivity are evaluated for air and the mass diffusion coefficient of each species is evaluated by assuming binary diffusion with air. All of the properties vary with temperature. We neglect the effects of the solid particles on the gas phase flow field, pressure work, dissipation and the interdiffusion of species terms in the energy equation.

Particle concentration equation:

$$\sqrt{g}(C)_t + [\sqrt{g}(U^i_{EFF} C)]_{\xi^i} - \sqrt{g}\omega_2 M_{SiO_2} = 0. \tag{10}$$

Here C is the mass concentration of the SiO_2 particles and M_{SiO_2} denotes the molecular weight of SiO_2. The particles are small and the effects of Brownian diffusion are neglected with respect to thermophoretic transport (Homsy *et al.* [3], Batchelor and Shen [4]). The velocities of the particles, U^i_{EFF} are equal to the sum of the gas and the thermophoretic velocities (Homsy *et al.* [3], Talbot *et al.* [17]); i.e.

$$U^i_{EFF} = \vec{a}^i \cdot (u_{EFF}\vec{i} + v_{EFF}\vec{j}) \tag{11}$$

where

$$u_{EFF} = u - K\frac{v}{T}\frac{\partial T}{\partial x}, \quad v_{EFF} = v - K\frac{v}{T}\frac{\partial T}{\partial y}. \tag{12}$$

The value of the thermophoretic coefficient K is equal to 0.55 (Kim and Pratsinis [14]).

2.2. *Boundary conditions*

On A′–A which is the transformed cylinder surface, the no-slip boundary condition for the velocity is used. The wall temperature is constant on A′–A. The normal-derivatives of the particle concentration and mass fractions are taken to be zero on the wall, i.e. $\partial C/\partial n = 0$ and $\partial Y_l/\partial n = 0$ on A′–A. B′–A′ and A–B represent the branch cut and the velocities, temperature, mass fractions and particle concentration along these two boundaries are identical. The stream wise second derivatives of the variables on B′–C′ and B–C, which are located far downstream, are assumed to be zero. On the boundaries C′–D′, D′–E′, E–D and D–C, it is assumed that the flow is particle free, the temperature and mass fractions are at the constant ambient values and the properties are evaluated as air. On the boundary C′–D′ and D–C which is far from the cylinder, $\partial v/\partial y = 0$. The entrained flow on these boundaries is assumed to be irrotational, $\partial^2 u/\partial y^2 = 0$. On the upstream boundary D′–E′ and E–D, the entrained flow is assumed to be perpendicular to the axis of the jet, i.e. $u = 0$ and $\partial v/\partial y = 0$. The velocities and temperature are uniform on E′–E corresponding to the jet exit, i.e. $u = U_j$, $v = 0$ and $T = T_j$.

2.3. *Deposition flux and deposition efficiency*

The local particle deposition flux at the wall, $J_w(\theta)$, is equal to the product of the normal component of the thermophoretic velocity $u_{th,w}(\theta)$ and the particle mass concentration $C_w(\theta)$:

$$J_w(\theta) = u_{th,w}(\theta) C_w(\theta). \tag{13}$$

The deposition efficiency η is defined as the ratio of the total deposition rate, F_w to the total particle production rate which is obtained stoichiometrically from the inlet mass flow rate of $SiCl_4$:

$$\eta = \frac{F_w}{\int_{-w_t}^{w_t} U_j C_{SiCl_4} \, dy} \frac{M_{SiCl_4}}{M_{SiO_2}} \tag{14}$$

where

$$F_w = 2\pi R \bar{J}_w, \bar{J}_w = \frac{1}{2\pi}\int_{-\pi}^{\pi} J_w(\theta) \, d\theta.$$

3. NUMERICAL METHOD

3.1. *Numerical procedure*

The governing equations (4)–(7) and (9) can be written in a generalized form according to

$$\sqrt{g}(\rho\phi)_t+[\sqrt{g}(\rho U^i\phi-\Gamma g^{ij}\phi_{\xi^j})]_{\xi^i}-b=0 \quad (15)$$

where ϕ denotes an arbitrary variable. To discretize the equations, the backward Euler method is used in the time domain. Due to the non-linearity of the exponential terms in the reaction rates, explicit reaction terms in the energy and species equations are used to avoid oscillation. Since Reynolds numbers are not large, the convection-diffusion discretization equations are obtained using the HYBRID scheme (Patankar [18]). The discretized form of the equation in the control volume is written as

$$A_P\phi_P=A_N\phi_N+A_S\phi_S+A_E\phi_E+A_W\phi_W+S_\phi. \quad (16)$$

The coefficients A_i are the integrated convective and diffusive fluxes across the surface of the control volume and the subscripts N, S, E and W denote the four neighboring grid points about P. S_ϕ includes non-orthogonal terms and all the terms proportional to the control volume.

The SIMPLE algorithm (Patankar [18]) is used to solve the flow field. A non-staggered grid system is chosen. To avoid a 'zigzag' pressure field [18], the velocities, U^i, on the surface of the control volume which determine the convection terms are obtained by solving linearized momentum equations [10, 16, 19, 20].

A Modified Strongly Implicit (MSI) method (Schneider and Zedan [21]) is adopted to solve the discretization equations. The solution is iterative in nature and is considered to be converged when the sum of the dimensionless residuals of the variables over the domain is less than 10^{-5}. The time step used for the calculation is equal to 0.001 s. The steady state solution is obtained by continuing in time until the solution changes less than 0.1% in successive time steps. Calculations were compared with the results of Kang and Greif [10, 16] and excellent agreement was obtained. Typically, differences were less than 3% for the Nusselt number and less than 1% for the friction.

3.2. *Computational domain*

The downstream location B′–C′ and B–C is chosen to be at $20R$. The external boundaries C′–D′ and C–D are located at $\pm 10R$ (Kang and Greif [10, 16]). The grids are non-uniform and more closely spaced near the cylinder surface and the burner. Grid points of 111×41 in the ξ and η directions are used in the calculations. The typical computing time is sixteen hours on a DEC 5000 125 workstation.

4. RESULTS AND DISCUSSION

4.1. *Scope of study*

Important parameters include the radius of the cylinder, R, the distance between the torch and the stagnation point, L, the eccentricity of the torch relative to the cylinder, E, and the rotational speed of the cylinder, Ω. The values used for the calculations are:

$$R = 0.0078, 0.0100^*, 0.0140 \text{ (m)}$$

$$L = 0.0500, 0.0600, 0.0700^*, 0.0800, 0.0900 \text{ (m)}$$

$$E = 0.0000^*, 0.0005, 0.0010, 0.0015 \text{ (m)}$$

$$\Omega = 0^*, 60, 120, 300 \text{ (rpm)}.$$

The nominal values are starred. The velocity and the temperature of the jet at the exit are equal to 2 m s^{-1} and 1200 K, respectively, and the ambient temperature T_a is 300 K. Calculations were carried out for uniform cylinder wall temperatures, T_w, of 1000, 1200 and 1400 K. The equivalence ratios for methane and for silicon tetrachloride oxidation are 0.6 and 1.0, respectively.

4.2. *Flow pattern, heat and mass transfer*

The velocity vectors and the temperature contours for the nominal values of the variables are shown in Figs. 2(a) and (b). Temperature profiles at different axial locations are shown in Fig. 3(a). The gases emerge from the burner and accelerate due to the decrease in the density and to the effects of buoyancy. The energy release from the oxidation of methane increases the temperature and there is then a diffusion of energy away from the oxidation region to the center; i.e. inward and also outward. This causes the centerline temperature to increase downstream while the maximum temperature decreases. The velocity is smaller at the center than in the higher temperature region surrounding the center. As the jet approaches the cylinder, the flow spreads laterally and a boundary layer is formed over the surface of the cylinder. The variation of the friction over the surface is shown in Fig. 3(b). The non-dimensional length from the rear stagnation point to the location where the velocity is zero, L_s/R, is equal to 0.72. Separation occurs at $\theta = 163.4^\circ$.

The distributions of the mass concentrations of $SiCl_4$ and SiO_2 at different axial locations are shown in Fig. 4(a). The mixture of silicon tetrachloride and oxygen which emerges from the central channel spreads laterally and reacts to form the SiO_2 particles. The maximum concentration of $SiCl_4$ is on the center line and decreases downstream; correspondingly, the SiO_2 particle concentration increases downstream. The particles begin to form at about $x = 2$ cm and the concentration of $SiCl_4$ becomes almost zero at $x = 6$ cm. It is found that the reaction is complete and no $SiCl_4$ is present when the temperature is greater than 2000 K (Kim and Pratsinis [14]). The particles are formed in the high temperature zone next to the central region and move inward to the lower temperature region due to the thermophoretic force. At $x = 3$, 4 and 5 cm, the maximum particle concentrations are away from the center while at $x = 6$ cm the maximum particle concentration is at the center.

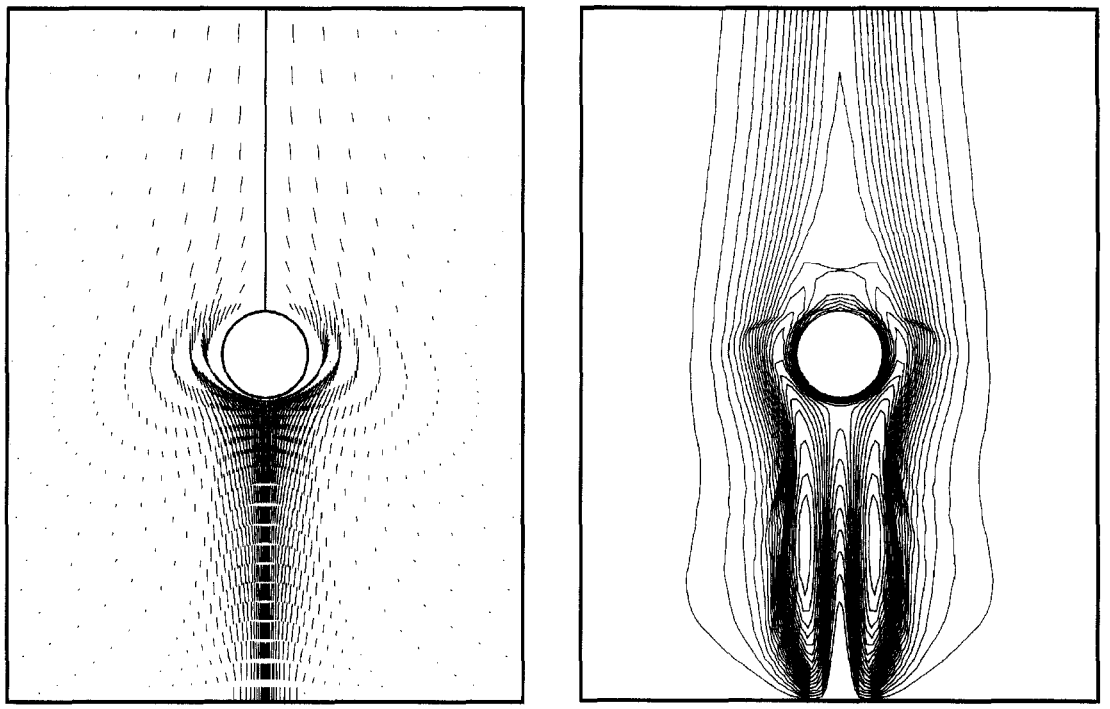

Fig. 2. (a) Velocity vectors; $R = 1$ cm, $L = 7$ cm. (b) Temperature contours; $R = 1$ cm, $L = 7$ cm.

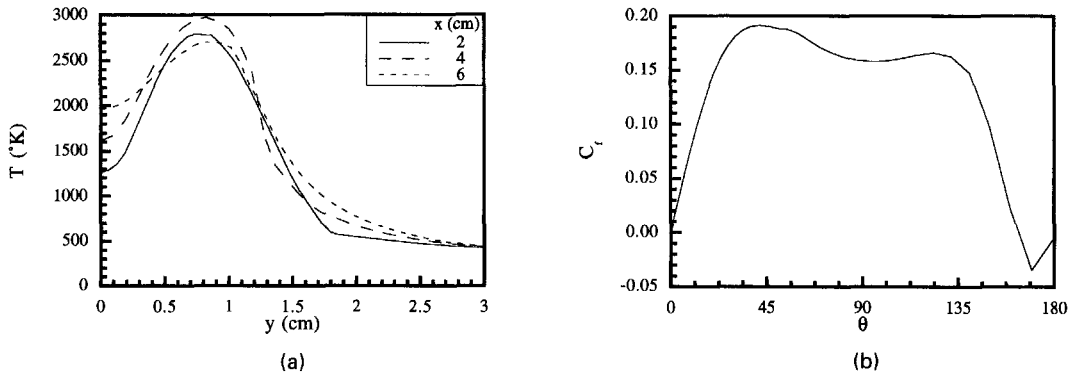

Fig. 3. (a) Temperature profiles at three different axial locations; $R = 1$ cm, $L = 7$ cm. (b) Variation of the skin-friction coefficient over the cylinder; $R = 1$ cm, $L = 7$ cm.

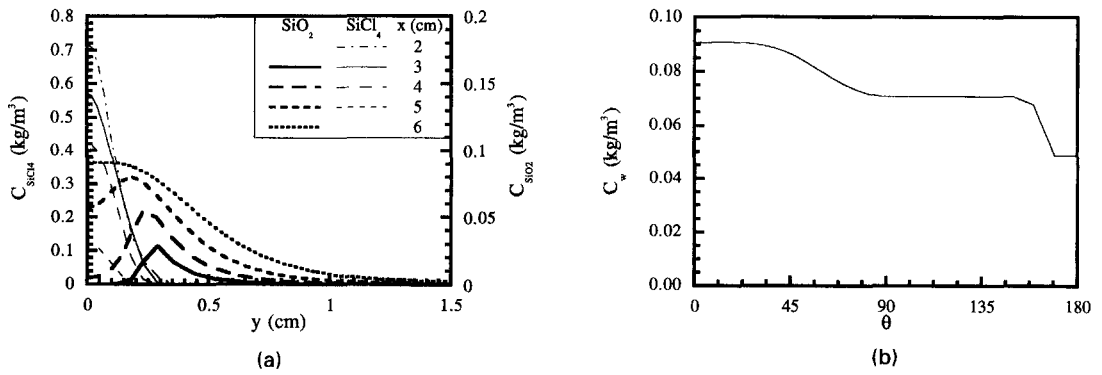

Fig. 4. (a) Distributions of mass concentrations of $SiCl_4$ and SiO_2 at different axial locations; $R = 1$ cm, $L = 7$ cm. (b) Variation of the mass concentration of SiO_2 over the cylinder; $R = 1$ cm, $L = 7$ cm.

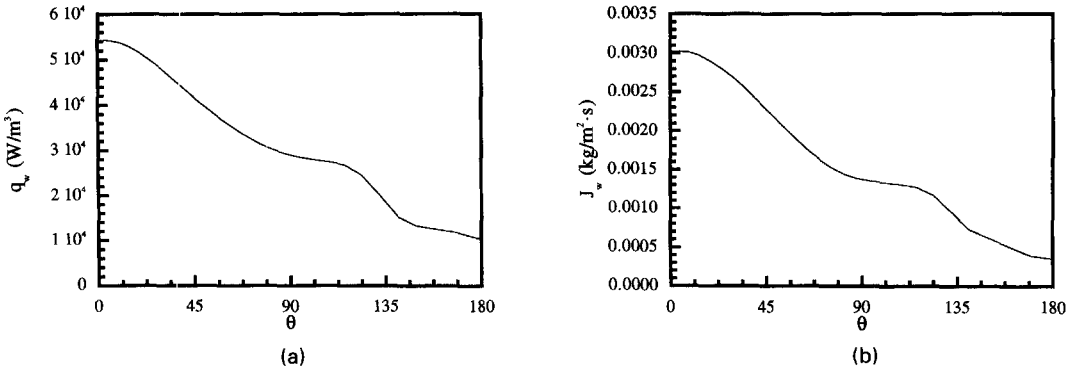

Fig. 5. (a) Variation of the heat flux over the cylinder; $R = 1$ cm, $L = 7$ cm. (b) Variation of the deposition flux over the cylinder; $R = 1$ cm, $L = 7$ cm.

The particle mass concentration distribution on the surface of the cylinder is shown in Fig. 4(b) for the nominal values of the variables. The particle concentration is a maximum at the stagnation point; note that the concentration is much smaller in the recirculation region.

The wall heat flux distribution is shown in Fig. 5(a); the heat flux is a maximum at the stagnation point and decreases as ϑ increases. The velocities of the particles are equal to the sum of the gas and the thermophoretic velocities. At the surface the velocities of the particles are equal to the thermophoretic velocities. The normal component of the particle velocity on the cylinder surface is proportional to the radial temperature gradient [or surface heat flux, $q_w(\theta)$]. Thus the deposition flux $J_w(\theta) = u_{th,w}(\theta)C_w(\theta) \sim q_w(\theta)C_w(\theta)$ [Abbott, J. S. personal communication (1993)]; note that the temperature on the cylinder surface is constant. The deposition flux is a maximum at the stagnation point and decreases around the cylinder [cf. Fig. 5(b)].

4.3. *Effect of the diameter of the target*

The deposition efficiency increases for increasing diameter of the cylindrical target over the range studied [$D < 3$ cm, Fig. 6(a)]. For increasing diameter, the target deposition area is larger and the efficiency is higher. It is noted that the size of the cylinder does not significantly affect the upstream reaction zone where the particles are formed. It is pointed out that the experimental values are for three dimensional deposition on a long cylindrical target with a round jet emerging from a 1.7 cm diameter burner and $L = 7.5$ cm [7, Bautista, J. R. personal communication (1992)]. The experiment has important variations of the temperature and deposition along the axial direction of the target which are not present in the two-dimensional (2D) calculations (which have no axial variation). The variation in the axial direction has been pointed out by Graham and Alam [8]. The experimental data are apparently overall results over the total axial length of the cylindrical target.

It is emphasized that the present 2D study would correspond to a burner that is very long in the axial direction of the target (cylinder). It is therefore not surprising that there is a large difference between the present 2D results and the data from the 3D experiment (for a finite burner with strong variation in the axial direction); cf. Graham and Alam [8].

4.4. *Effect of the wall temperature*

The variation of deposition efficiency for different wall temperatures is shown in Fig. 6(b). The deposition efficiency increases from 15 to 20% as the wall

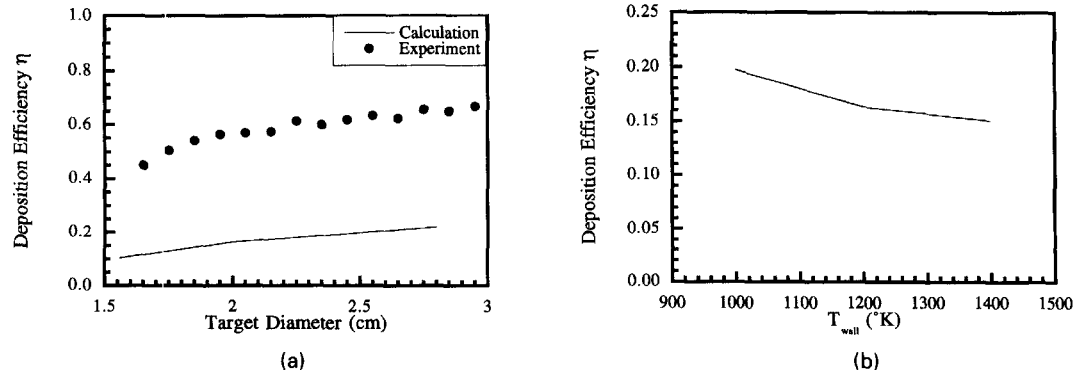

Fig. 6. (a) Effect of target diameter on deposition efficiency; $L = 7$ cm. Experiments are in a three-dimensional system (Bautista *et al.* [7]). (b) Effect of wall temperature on deposition efficiency; $R = 1$ cm, $L = 7$ cm.

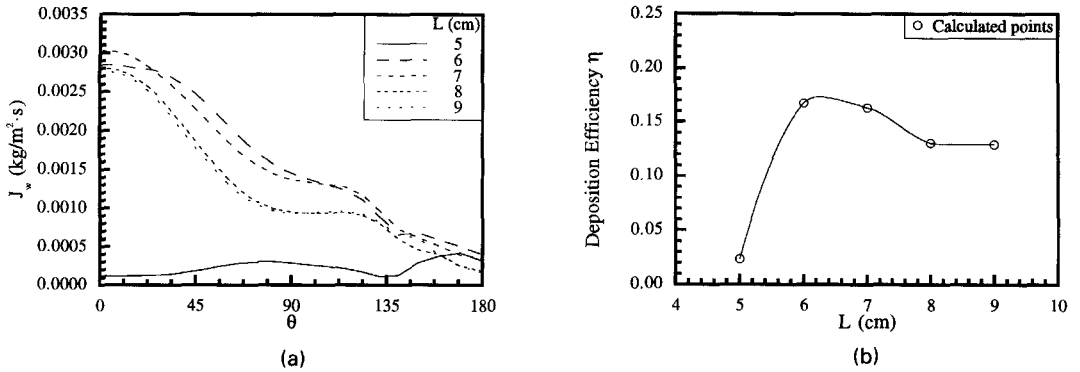

Fig. 7. (a) Variation of the deposition flux over the cylinder; $R = 1$ cm. (b) Variation of the deposition efficiency with separation distance; $R = 1$ cm.

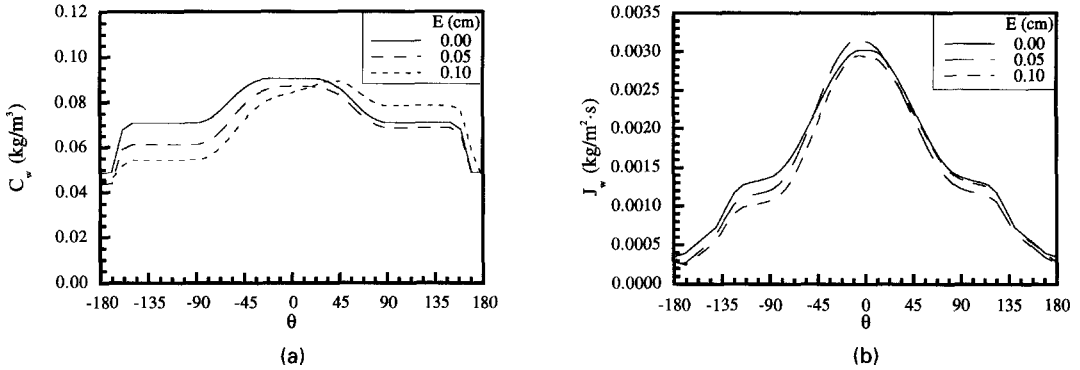

Fig. 8. (a) Variation of the particle mass concentration over the cylinder; $R = 1$ cm, $L = 7$ cm. (b) Variation of the deposition flux over the cylinder; $R = 1$ cm, $L = 7$ cm.

temperature decreases from 1400 to 1000 K. For lower wall temperatures, the deposition fluxes are larger due to the larger thermophoretic velocities which result in the higher deposition efficiency.

4.5. *Effect of the separation distance* L

The variation of the deposition flux on the cylinder surface, $J_w(\theta)$, and the deposition efficiency, η, for different separation distances between the burner and the target are shown in Figs. 7(a) and (b), respectively for a 2 cm target diameter. For $L = 5$ cm, silicon tetrachloride is not depleted by the time the flow reaches the target and the deposition flux and efficiency are low [Fig. 4(a) shows that the concentration of $SiCl_4$ becomes negligible at $x = 6$ cm for a separation distance $L = 7$ cm]. For $L = 6$ cm the deposition flux and efficiency are a maximum. For $L > 6$ cm, the temperature gradient and the particle mass concentration on the cylinder surface decrease for increasing L which causes the deposition flux and efficiency to decrease (with increasing L). The three dimensional experiments of Graham and Alam [8] also show a maximum in the efficiency for moderate L. It is also pointed out that their experiments utilize a different burner than is studied in the present work.

4.6. *Effect of the eccentricity of the burner*

The particle mass concentration on the wall, $C_w(\theta)$, is shown in Fig. 8(a) for different eccentricities, E. The effect of eccentricity results in an asymmetric distribution although for the values of E studied; i.e. $E \leqslant 0.15$ cm (corresponding to Bautista *et al.* [7]) the numerical values of the particle concentration and the deposition flux distributions vary only slightly with respect to E [Fig. 8(b)]. Figure 9 shows the deposition

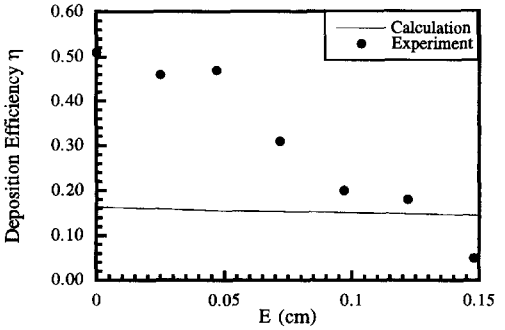

Fig. 9. Variation of the deposition efficiency with eccentricity; $R = 1$ cm, $L = 7$ cm. Experiments are in a three-dimensional system (Bautista *et al.* [7]).

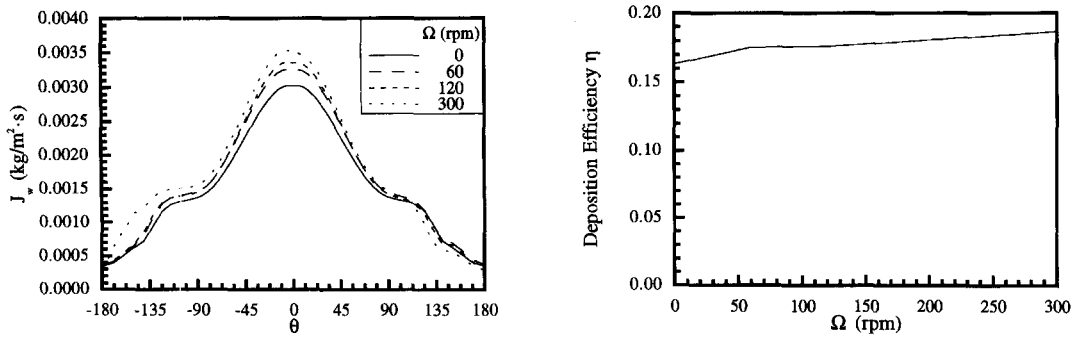

Fig. 10. (a) Variation of the deposition flux; $R = 1$ cm, $L = 7$ cm. (b) Variation of the deposition efficiency with rotational speed; $R = 1$ cm, $L = 7$ cm.

efficiency as a function of the eccentricity E; in particular, results from the calculations for the two-dimensional (2D) configuration and from the 3D experiments of Bautista *et al.* [7] are shown. The calculated efficiency decreases only slightly as the eccentricity increases because the distribution of the SiO_2 particles near the cylinder is fairly uniform [Fig. 4(a)] and thus is relatively insensitive to the eccentricities (for $E \leqslant 0.15$ cm). The three dimensional experiments, however, show a large decrease of the efficiency with respect to increasing eccentricity.

4.7. *Effect of the rotational speed of the target*

The deposition flux distributions for different rotational speeds of the cylinder are shown in Fig. 10(a). The rotation of the cylinder increases the heat flux and the deposition flux on the surface of the cylinder and changes the locations of the separation points. The increase in deposition efficiency for increasing rotational speed is shown in Fig. 10(b).

5. CONCLUSIONS

Numerical solutions have been obtained for the flow, heat and mass transfer, and particle deposition resulting from the impingement of a plane reacting jet on a cylinder. The following conclusions are drawn:

(1) The temperature of the jet increases due to methane oxidation with the maximum temperatures occurring near the ring containing the methane-oxygen mixture. Silicon dioxide particles are formed from the oxidation of silicon tetrachloride which is activated by the energy release from the oxidation of methane.

(2) Silicon dioxide particles are formed in the hot region and diffuse inward due to thermophoresis. The transverse distributions of the particles vary with the axial location.

(3) The deposition efficiency increases as the diameter of the cylinder increases.

(4) The distance between the burner and the target is an important parameter for the deposition efficiency. An optimum value of 6 cm is obtained.

(5) Over the range of eccentricities of the burner from 0 to 0.15 cm there is only a slight effect on the calculated deposition efficiency for a two dimensional system. Measurements in a three dimensional system (Bautista *et al.* [7]) exhibit a large decrease in efficiency for increasing eccentricity.

(6) Rotation of the target increases the deposition efficiency.

Acknowledgements—Support from the National Science Foundation is gratefully acknowledged. The research is part of a joint program with Professor J. W. Daily of the University of Colorado on chemical vapor deposition processes. The authors are indebted to Professors J. W. Daily and J. Hwang for helpful discussion.

REFERENCES

1. T. Li, *Optical Fiber Communications*. Academic Press, New York (1985).
2. J. R. Bautista and R. M. Atkins, The formation and deposition of SiO_2 aerosols in optical fiber manufacturing torches, *J. Aerosol Sci.* **22**(5), 667–675 (1991).
3. G. M. Homsy, F. T. Geyling and K. L. Walker, Blasius series for thermophoretic deposition of small particles, *J. Colloid Interface Sci.* **83**(2), 495–501 (1981).
4. G. K. Batchelor and C. Shen, Thermophoretic deposition of particles in gas flowing over cold surfaces, *J. Colloid Interface Sci.* **107**(1), 21–37 (1985).
5. V. K. Garg and S. Jayaraj, Thermophoretic deposition over a cylinder, *Int. J. Engng Fluid Mech.* **3**(2), 175–196 (1990).
6. V. K. Garg and S. Jayaraj, Thermophoretic deposition in crossflow over a cylinder, *J. Thermophys.* **4**(1), 115–116 (1990).
7. J. R. Bautista, K. L. Walker and R. M. Atkins, Modeling of heat transfer and mass transfer in the manufacture of optical waveguides, *A.I.Ch.E. Natn. Meeting*, Washington, DC (1988).
8. G. M. Graham and M. K. Alam, Experimental study of the outside vapor deposition process, *Aerosol Sci. Technol.* **15**, 69–76 (1991).
9. M. K. Alam, G. M. Graham, V. Janakiraman and J. Greaves, Numerical analysis of thermophoretic transport in the OVD process, *ASME Numer. Heat Transfer*, HTD-Vol. 130, 67–72 (1990).
10. S. H. Kang and R. Greif, Thermophoretic transport in the outside vapor deposition process, *Int. J. Heat Mass Transfer* **36**(4), 1007–1018 (1993).
11. H. C. Tsai and R. Greif, Thermophoretic transport with

application to external vapor deposition processes, *Int. J. Heat Mass Transfer* **37**(2), 257–268 (1994).
12. H. C. Tsai, R. Greif and S. Joh, A study of thermophoretic transport in a reacting flow with application to external chemical vapor deposition processes, *Int. J. Heat Mass Transfer*, submitted for publication.
13. C. K. Westbrook and F. L. Dryer, Simplified reaction mechanisms for the oxidation of hydrocarbon fuels in flames, *Combustion Sci. Technol.* **27**, 31–43 (1981).
14. K. S. Kim and S. E. Pratsinis, Manufacture of optical waveguide preforms by modified chemical vapor deposition, *A.I.Ch.E. Jl* **34**(6), 912–920 (1988).
15. J. F. Thompson, Z. A. Warsi and C. W. Mastin, *Numerical Grid Generation, Foundations and Applications*. North-Holland, New York (1985).
16. S. H. Kang and R. Greif, Flow and heat transfer to a circular cylinder with a hot impinging air jet, *Int. J. Heat Mass Transfer* **35**(9), 2173–2183 (1992).
17. L. Talbot, R. K. Cheng, R. W. Schefer and D. R. Willis, Thermophoresis of particles in a heated boundary layer, *J. Fluid Mech.* **101**(4), 737–758 (1980)
18. S. V. Patankar, *Numerical Heat Transfer and Fluid Flow*. Hemisphere, New York (1980).
19. M. J. Schuh, Numerical prediction of fluid and particle motions in flows past tubes, Ph.D. Thesis, University of California, Berkeley (1987).
20. M. J. Schuh, C. A. Schuler and J. A. C. Humphrey, Numerical calculation of particle-laden gas flows past tubes, *A.I.Ch.E. Jl* **35**(3), 466–480 (1989).
21. G. E. Schneider and M. Zedan, A modified strongly implicit procedure for the numerical solution of field problems, *Numer. Heat Transfer* **4**, 1–19 (1981).